COMSOL
CONFERENCE
2024 FLORENCE

Modeling an Open-Cell Foam Heat Exchanger

B. Chiné[1], F. Rodriguez-Mendez[1], M. Meneses-Guzman[2]
1. School of Materials Science and Engineering, Costa Rica Institute of Technology, Cartago, Costa Rica.
2. School of Industrial Production Engineering, Costa Rica Institute of Technology, Cartago, Costa Rica.

Abstract
Metal foams are interesting materials with many potential uses, characterized by a cellular structure represented by a metal (or a metal alloy) and gas voids inside. A common metallic cellular material is an open-cell metal foam, considered to have very promising properties to improve efficiency and minimize the required weight and volume of novel industrial heat exchangers.
In this work we use COMSOL Multiphysics® 6.2 to model fluid flow and heat transfer in a 3D heat exchanger prototype. In the device, a 40 PPI (pores per linear inch) open-cell foam has been bonded to cylindrical tubes carrying hot water, to improve the heat transfer with a cold air stream. In the model, heat is transferred by convection and diffusive mechanisms in the fluids and by conduction in the solid regions of the system. The weakly compressible air flow through the porous copper foam, modelled by the Brinkman equations, and the water flow in the tubes are both assumed as laminar and coupled to the heat transfer mechanisms. The copper sponge is represented as a porous medium in the local thermal non-equilibrium interface, using its properties and specifying the interstitial convective heat transfer coefficient.
The computational results prove that the energy transfer is enhanced due to the copper sponge's high porosity and large specific surface area. However, despite of the improved heat transfer experimented by the air, the reduction of water temperature is low, also constrained by the short tube length. These results have been confirmed with experimental work and show that the computational model, developed with COMSOL Multiphysics®, is effective for modelling the conjugate heat transfer process of the open-cell foam heat exchanger.

Keywords: Open-cell foam, heat exchanger, Brinkman equations, heat transfer in porous media.

1. Introduction
Open-cell metal foams (or metal sponges) are interesting materials with many potential uses [1]. These materials can be used to enhance heat transfer in many applications, such as cryogenic heat exchanger, compact heat sinks and heat exchanger, as remarked by Lu et al. [2]. They are characterized by a cellular structure represented by a metal (or a metal alloy) and connected gas voids inside (Fig. 1). Due to their intrinsic high porosity and large specific surface area [3], these materials are considered to have very promising properties to improve efficiency and minimize the required weight and volume of novel industrial heat exchangers. However, the complexity of the convective heat transfer process, and the number of parameters to analyze simultaneously, demand a preliminary and hugely wide experimental activity to design foamed components with a good quality for energy transferring systems. The development of computational models may help to reduce experimental work and costs, although the task is very challenging. Numerical modelling of porous media has been used to capture the details of the intricate sponge structure while considering the porous solid-fluid systems as homogeneous [4]. Moreover, computational attempts modelling representative elementary volume (REV) of a sponge with its solid and void phases have also shown encouraging results [3,4,5]. Interesting computational models based on X ray micro-tomographic scans of the sponge geometry have been developed by many authors, among others

Figure 1. An open-cell copper foam.

Meinicke et al. [6], Dixit and Gosh [7] and Jafarizade et al. [8]. Bayomy and Saghir [9] investigated the heat transfer characteristics of aluminum foam heat sink for electronic devices cooling, developing three different geometries of the sink. The authors used the software COMSOL Multiphysics® to evaluate and successfully compare the distributions of temperature, Nusselt numbers and pressure drops of the three sinks. On the other hand, Bidar et al. [10] developed a computational model of forced convective heat transfer to study the airflow through a two-sided vertical channel filled with open-cell metal foams. Odabaee and Hooman [11] reported numerical results on the reduction of the air-side thermal resistance from a four-row heat exchanger, containing aluminium tubes wrapped by metal foam in crossflow. Mancin et al. [12] measured experimental heat transfer coefficients by means of

an experimental work, which considered air flow heating in different aluminum open-cell foam samples, under a wide range of air mass velocity. More recently, Assan et al. [13] numerically studied the dynamic and thermal performance of a heat exchanger composed of copper foam incorporated in a fan coil. Yang et al. [14] calculated the interstitial heat transfer coefficient for air-foam system using pore-scale simulation, under local thermal non-equilibrium conditions (LTNE) in rotating machines. The Darcy–Forchheimer model and the LTNE model have been used to describe the momentum and energy transfer in metal foams [15,16]. Finally, the flow characteristics, such as permeability and inertial coefficient, during forced convection in internal flow, have been obtained by Roge et al. [17] from pressure drop measurements.

In this work, we use COMSOL Multiphysics® 6.2 to model fluid flow and heat transfer processes through a compact open-cell foam heat exchanger. In the device, heat is transferred from a stream of hot water to a cold air flow. The study takes in consideration convection and diffusive mechanisms in the fluids and conduction in the solid regions of the system.

The structure of the paper is the following. The description of the physical model and the governing equations are given in Section 2, whereas Section 3 describes the use of COMSOL Multiphysics®. Finally, the computational results are presented in Section 4 and the conclusions in Section 5.

2. Model

2.1. Physical model

Fig. 2 shows a 3D view of the compact heat exchanger while Table 1 gives its main geometrical dimensions. The total length L is 230 mm, the width W is 101.6 mm, the height H is 50.8 mm, and the wall thickness is 5 mm. The central parallelepipedal region of the device is joined to two end sections, with a decreasing cross section (Fig. 3) to connect the cylindrical air inlet and outlet tubes of inner diameter D_a, equal to 21.54 mm. Also, there are three cylindrical copper tubes with an inner diameter D_w of 4.35 mm centrally located in the device, enabling the crossflow of water respect to the air flow. Sandwiched to the external surface of the three water tubes, there are two identical 40 PPI (pores per linear inch) open-cell copper foams of dimensions 101.6x50.8x12.7 mm^3, as indicated in Fig. 4. The properties of the open-cell foams manufactured by ERG Aerospace Co. (Oakland, CA, USA) from a C10100 copper alloy, are given in Table 2.

We start our modelling work by importing in COMSOL Multiphysics® the geometry of the heat

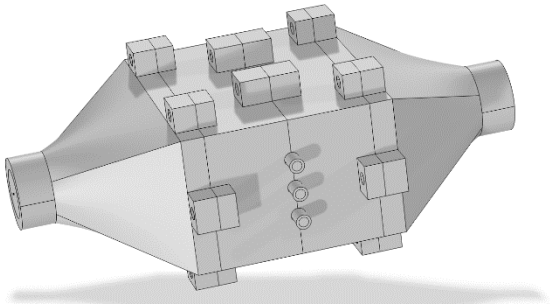

Figure 2. The compact heat exchanger.

***Table 1**. Dimensions of the compact heat exchanger.*

Magnitude	*Value*
Length L	230 mm
Width W	101.6 mm
Height H	50.8 mm
Wall thickness t	5 mm
Inner diameter D_a of air inlet and outlet	21.54 mm
Inner diameter of the copper tubes for the water crossflow	4.35 mm
Copper sponge width w	101.6 mm
Copper sponge height h	50.8 mm
Copper sponge thickness s	12.7 mm

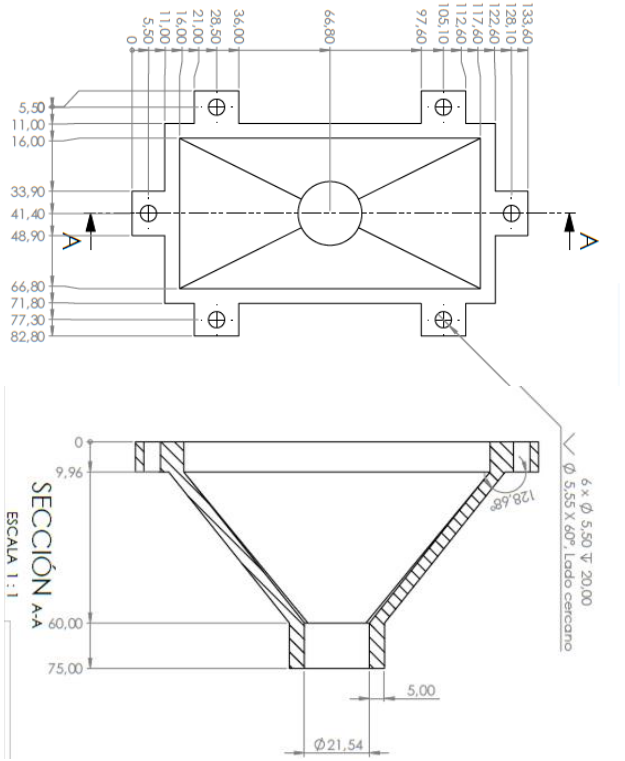

Figure 3. Dimensions of the compact heat exchanger´s end sections to connect the air inlet and outlet.

exchanger generated with SolidWorks®. It is important to highlight that the heat exchanger is symmetrical with respect to the *y*-*z* plane (Fig. 5), therefore the computational domain can be reduced, as shown in the same figure. In the device, the cold air flows longitudinally in the *y* direction, whereas the water is fed by a crossflow configuration in the *z* direction.

2.2. Governing equations

The weakly compressible cooling air flow through the heat exchanger, and the incompressible hot water flow into the cylindrical tubes are both assumed as steady state and laminar and then coupled to the heat transfer mechanisms. In addition, the region of the open-cell copper foam is modelled as a porous medium with non-Darcian flow and in local thermal non-equilibrium conditions, therefore the solid and the fluid temperature are not in equilibrium. Consequently, the governing equations are the mass conservation and the linear momentum conservation described by the Navier-Stokes equations and the conservation of the thermal energy, represented by the Fourier equation with convective terms for the fluid region. For a steady state process, in vector form they can be read as, respectively [18,19]

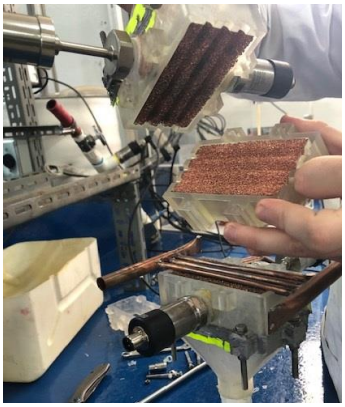

Figure 4. View of two open-cell copper foams to sandwich to the external surfaces of three copper tubes (shown down in the picture).

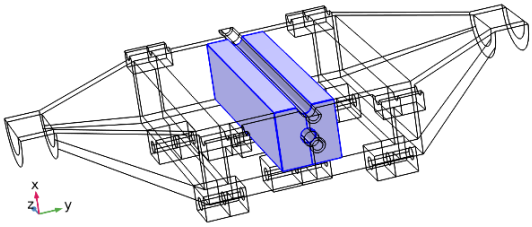

Figure 5. A view of the compact heat exchanger reduced by symmetry, with the central region representing the copper foam joined to the hot water tubes.

***Table 2**. Properties of the copper open-cell foam.*

Magnitude	*Value*
Copper alloy	C10100
Pore density (pores per linear inch)	40
Relative density *RD*	10%
Specific heat	0.385 J/(g K)
Porosity ε_p	90%
Specific surface area S_b	24 in^2/ in^3
Total thermal conductivity	13.2 W/ (m K)
Permeability	1.6 x10^{-7} m^2
Interstitial heat transfer coefficient h_{sf}	140 W/ (m^2 K)

$$\nabla \cdot (\rho \mathbf{u}) = 0 \quad (1)$$

$$\rho(\mathbf{u} \cdot \nabla)\mathbf{u} = \nabla \cdot \left[-p\mathbf{I} + \mu\left[\nabla \mathbf{u} + \{\nabla \mathbf{u}\}^{\mathrm{T}}\right] - \frac{2}{3}\mu[\nabla \cdot \mathbf{u}]\mathbf{I}\right] + \mathbf{F} \quad (2)$$

$$\rho c_p \, \mathbf{u} \cdot \nabla \mathrm{T} + \nabla \cdot \mathbf{q} = Q \quad (3)$$

where ρ is the density (kg/m^3), $\mathbf{u}$ (m/s) is the velocity in a fluid domain, p (Pa) is the pressure, μ is the viscosity (Pa·s), $\mathbf{I}$ means the identity tensor, $\mathbf{F}$ are the volume external forces applied to the fluid (N/m^3), T (K) is the temperature, c_p corresponds to the specific heat capacity (J/(kg K)), $\mathbf{q}$ represents the heat flux (W/m^2), and Q is the heat source (W/m^3). For the porous medium, we use the Brinkman equations to compute fluid velocity and pressure fields under laminar flow regime, which includes a term in the momentum balance for the viscous transport. If ε_p is the porosity, κ (m^2) the permeability, and Q_m (kg/(m^3 ·s) a mass source or sink, the conservation of the linear momentum is [18]

$$\frac{\rho}{\varepsilon_p}(\boldsymbol{u} \bullet \nabla)\,\frac{\boldsymbol{u}}{\varepsilon_p} = -\nabla p + \nabla \bullet \left[\frac{1}{\varepsilon_p}\left\{\mu(\nabla \boldsymbol{u} + (\nabla \boldsymbol{u})^T - \frac{2\mu}{3}(\nabla \bullet \boldsymbol{u})\boldsymbol{I}\right\}\right] - \left[\kappa^{-1}\mu + \rho\beta|\mathbf{u}| + \frac{Q_m}{{\varepsilon_p}^2}\right]\mathbf{u} + \mathbf{F} \quad (4)$$

where the magnitude $-\rho\beta|\mathbf{u}|\mathbf{u}$ represents the viscous Forchheimer drag force, and β is a parameter depending on the porous medium permeability.
Furthermore, to compute the temperature field in the porous foam domain, we assume a non-equilibrium heat transfer, which for binary systems of rigid porous matrix and fluid phase is governed by a set of two equations. These are the usual heat equations for solids and fluids (Eq. 3), multiplied by the volume fractions $1 - \varepsilon_p$ and ε_p, respectively. To quantify the exchanged heat between both phases, named with q_{sf} the interstitial convective heat transfer coefficient, we use the additional source term

$$q_{sf}\,(T_s - T_f) \quad (5)$$

$$q_{sf}\,(T_f - T_s) \quad (6)$$

for the thermal energy balance of the fluid and solid phase, respectively.

2.3. Boundary conditions

Table 3 gives the physical properties for both the air inflow and water inflow of the computational model, also using the data of Bergman et al. [20]. Boundary conditions of no slip for the fluid flow are set on the solid walls confining the two fluids, air, and water. A thermal insulation restriction for the heat transfer is set on the external surfaces of the heat exchanger and a specific local thermal non-equilibrium boundary condition is used for the walls adjacent to the porous foam domain. Furthermore, no thermal resistance is considered between the copper tubes and the porous media. Finally, a symmetry condition is used for the central *y-z* longitudinal symmetry plane of the heat exchanger.

3. Solution with Comsol Multiphysics®

We study the steady state fluid flow and heat transfer processes through the 3D compact heat exchanger using the CFD [18] and Heat Transfer [19] modules of Comsol Multiphysics® 6.2, and modelling the open-cell foam as a Porous Medium. To couple the former physical mechanisms, we select the Conjugate Heat Transfer physics interface. In the model, heat is transferred from laminar streams of hot water to a laminar flow of cold air by convection and diffusive phenomena in the fluids. Also, heat conduction is considered in the solid regions of the system, consisting of exchanger walls, tubes walls and the solid foam matrix.

We assume the tube walls and the solid foam matrix as copper with density a of 8960 kg/m^3, thermal conductivity of 400 W/(m·K), and heat capacity at constant pressure of 385 J/(kg·K). For ε_p the porosity, κ (m^2) the permeability, β the parameter depending on the porous medium permeability, and h_{sf} (W/(m^2 K)) the interstitial heat transfer coefficient of the copper foam, we use the data of Table 2. The interstitial convective heat transfer coefficient q_{sf} is defined in Comsol Multiphysics® as the product of $S_b h_{sf}$.

The meshing strategy uses an unstructured free tetrahedral mesh in the air inlet and outlet sections, in the porous medium of the open-cell foam, and in the cylindrical tubes feeding the water flow. The rest of the device is divided in structured quadrilateral elements. The maximum element size is 3.94 mm, and the minimum element size is 0.744 mm, respectively equal to 2.75 mm and 0.298 mm for the cylindrical tubes of water. Fig. 6 shows a cross-sectional view of the mesh corresponding to the longitudinal *y-z* central plane of the heat exchanger. Also, boundary layers are created on the solid walls

***Table 3**. Experimental values used in the computational model.*

a) Air inflow

Magnitude	*Value*
Diameter D_a of the inlet area	21.54x10^{-3} m
Inlet area A_a	0.36440x10^{-3} m^2
Flow rate Q_a	23.408 L/min (0.39013x10^{-3} m^3/s)
Inlet velocity $U_{in,a}$	1.071 m/s
Temperature at inlet $T_{in,a}$	300 K
Density ρ_a (at 300K, 1atm)	1.1614 kg/m^3
Dynamic viscosity μ_a (at 300K, 1atm)	1.846x10^{-5} Pa·s
Heat capacity at constant pressure $c_{p,a}$ (at 300K, 1atm)	1.007 kJ/(kg·K)
Prandtl number Pr$_a$ (at 300K, 1atm)	0.707
Mass flow rate $\dot{m}_a = \rho_a U_{in,a} A_a$	0.4531x10^{-3} kg/s
Reynolds number $Re_a = \rho_a U_{in,w} D_a / \mu_a$	1451

b) Water inflow

Magnitude	*Value*
Diameter D_w of each tube	4.35x10^{-3} m
Inlet area A_w of each tube	0.14862x10^{-4} m^2
Total flow rate Q_w	1.893 L/min (0.31545x10^{-4} m^3/s)
Flow rate in each tube $Q_{in,w}$	0.10515x10^{-4} m^3/s
Inlet velocity $U_{in,w}$ in each tube	0.708 m/s
Temperature at inlet $T_{in,w}$	312 K
Density ρ_w (at 312 K, p_{sat})	992 kg/m^3
Dynamic viscosity μ_w (at 312 K, p_{sat})	0.669x10^{-3} Pa·s
Heat capacity at constant pressure $c_{p,w}$ (at 312 K, p_{sat})	4.178 kJ/(kg·K)
Prandtl number Pr (at 312K, p_{sat})	4.44
Mass flow rate in each tube $\dot{m}_w = \rho_w U_{in,w} A_w$	0.10431x10^{-1} kg/s
Total mass flow rate	0.31293x10^{-1} kg/s
Reynolds number at each inlet tube $Re_w = \rho U_{in,w} D_w / \mu_w$	4567

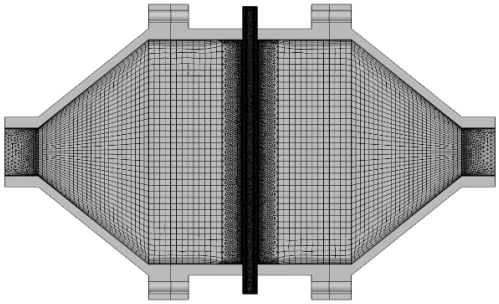

Figure 6. Cross-sectional view of the mesh on the central longitudinal y-z plane of the heat exchanger.

using default values of the software. Finally, the number of degrees of freedom (DFOs) to be solved for is 6.7×10^5 plus 6.0×10^4 internal DOFs, approximately.

4. Results and discussion

Initially, the computational results are displayed for an inlet air flow rate of 23.408 L/min at 300 K, and a water flow rate of 1.893 L/min at 312 K, according to Table 3. Figs. 7 and 8 shows the air temperature in the device and the velocity magnitude on a central longitudinal *y-z* plane, respectively. These results highlight that the temperature of the cold air increases as it flows through the open-cell foams and quickly achieves the value of 312 K, due to the sponge's high porosity and large specific surface area. The water temperature in the cylindrical crossflow tube doesn't show a significant variation, due to its higher heat capacity. These findings were confirmed by experimental measurements using the same heat exchanger. As shown in Fig. 8, there are two main recirculating streams between the central air jet and the solid walls of the heat exchanger, generating a specific pattern between velocity and temperature fields ahead of the open-cell foam.

Next, we analyze a heat exchanger with a second series of cylindrical tubes for the water flow. These identical tubes are placed downstream of the previous ones, raising the total number to six. The inlet air flow rate is again 23.408 L/min at 300 K, the water flow rate is the same of 1.893 L/min at 312 K, but the water velocity is now halved to 0.354 m/s, in each inlet tube. Figs. 9 and 10 plot, respectively, the new temperature and velocity arrows on the longitudinal central *y-z* plane and the temperature profile along the longitudinal *y* axis of the compact heat exchanger. We observe that the air temperature has practically approached 312 K behind the first series of hot water tubes, therefore there are not favorable conditions to transfer heat to air and again the water temperature doesn´t essentially change. To simulate the case of heat transfer with a hot fluid of lower heat capacity, we replace water with air at the same inlet temperature of 312 K. Fig. 11 gives the computed temperature field, showing that now the hot air quickly reduces its temperature to a value around 300 K, which is the inlet temperature of the cold air. Fig. 12 highlights that the air temperature along the *z* axis of the first central tube (placed on the middle of the exchanger) decreases until the

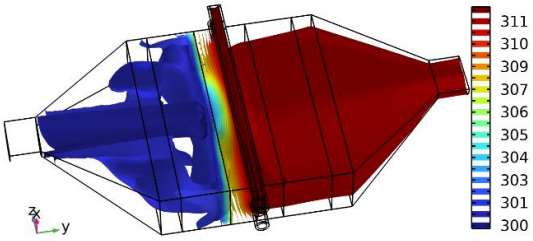

Figure 7. Temperature iso-surfaces (K) in the heat exchanger.

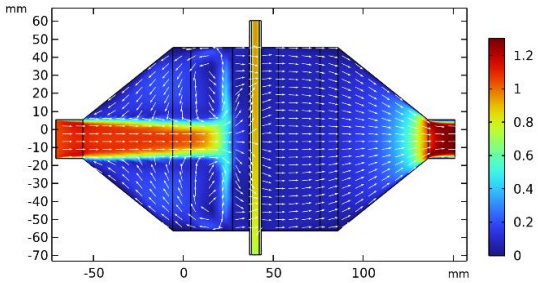

Figure 8. Velocity magnitude (m/s) and velocity arrows on the longitudinal central y-z plane.

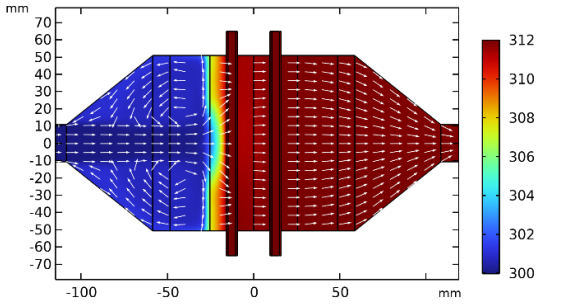

Figure 9. Temperature (K) and velocity arrows on the longitudinal central y-z plane (heat exchanger with 6 tubes for the water flow).

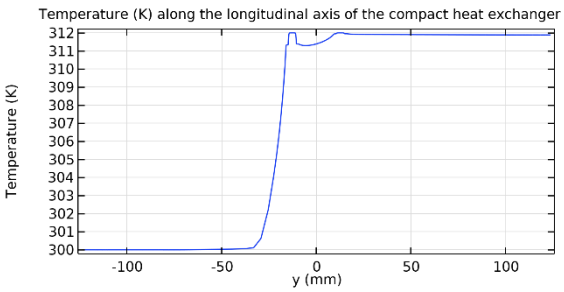

Figure 10. Temperature (K) along the longitudinal y axis of the heat exchanger, with 6 tubes for the water flow.

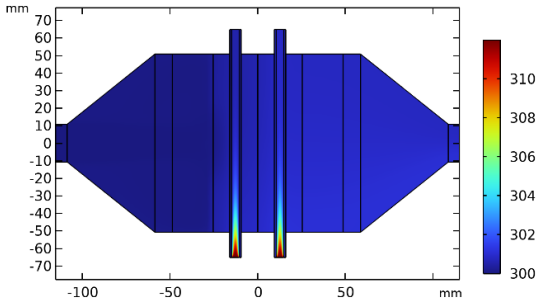

Figure 11. Temperature (K) on the longitudinal central z-y plane (heat exchanger with 6 tubes for air-air heat transfer).

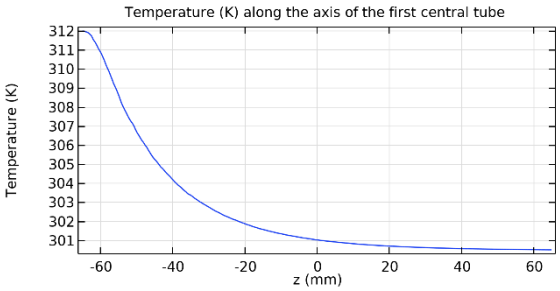

Figure 12. Temperature (K) along the z axis of the first central tube (heat exchanger with 6 tubes for air-air heat transfer).

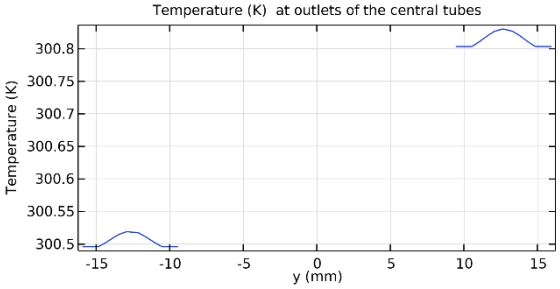

Figure 13. Temperature (K) at outlets of the central tubes (heat exchanger with 6 tubes for air-air heat transfer).

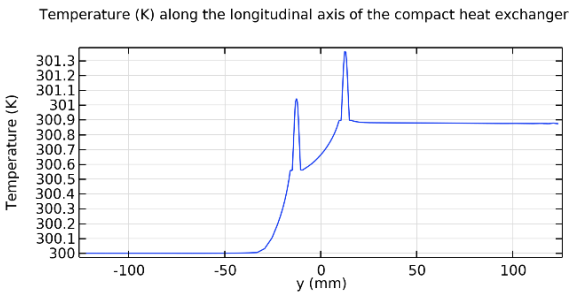

Figure 14. Temperature (K) along the longitudinal y axis of the heat exchanger, with 6 tubes for air-air heat transfer.

asymptotic value of 300 K, corresponding to the cold air temperature. The temperature profiles of Fig. 13 prove this for the hot air exiting from the outlets of the two central (median) tubes. As shown in Fig. 14, which depicts the temperature profile along the longitudinal *y* axis of the compact heat exchanger, now the cold air stream rises less its temperature when is flowing through the open-cell foams. Consequently, the cold air leaves the device with a temperature increase of 1 °C approximately, a much lesser value than 11 °C of Fig. 10, as computed before for the heat exchanger with water as hot fluid. The computational results demonstrate that the energy transfer of the exchanger is enhanced due to the copper sponge's high porosity and large specific surface area. As a verification, we plot in Fig. 15 the temperature field for the heat exchanger with three nude copper tubes for the water flow, without the open-cell foam. We observe that the cold air jet impacts the tubes, but the downstream air temperature is still around 300 K. Fig. 16 points out that the air temperature difference between the inlet and the outlet is approximately 3 °C, a very different result if compared to the previous case of Fig. 7 with copper sponges.

However, despite of the enhanced heat transfer experimented by the air, the reduction of the water temperature in the open-cell heat exchanger is low, mainly constrained by the short tube length and therefore requiring some geometrical improvements, as the introduction of coils or narrow channels to increase the resulting heat transfer surface.

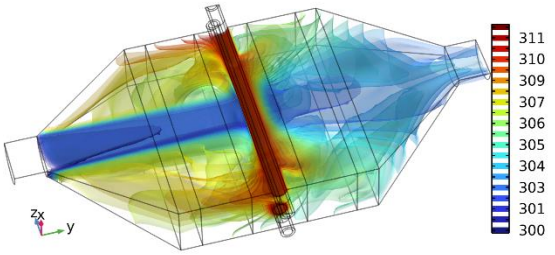

Figure 15. Temperature iso-surfaces (K) for the heat exchanger with 3 nude tubes, without open-cell foam.

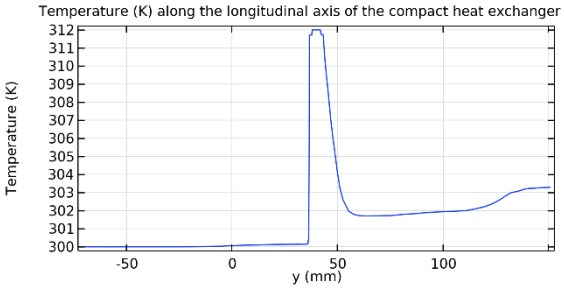

Figure 16. Temperature (K) along the longitudinal y axis of the heat exchanger with 3 nude tubes, without open-cell foam.

5. Conclusions

A computational model of the fluid flow and heat transfer in a 3D prototype of an open-cell foam heat

exchanger has been developed. In the device, a 40 PPI open-cell foam has been bonded to cylindrical tubes carrying hot water, to improve the heat transfer with a cold air stream. The numerical findings of the simulations show that the energy transfer of the exchanger is enhanced owing to the copper sponge's high porosity and large specific surface area. However, despite of the improved heat transfer experimented by the air, the reduction of water temperature in this compact device is low, also constrained by the short tube length and therefore requiring some different components, such as coils or narrow channels. Nevertheless, the previous results show that the computational model developed with COMSOL Multiphysics® is effective for modelling the conjugate heat transfer process of this compact device. We foresee a future series of computational efforts to study novel solutions for open-cell foam heat exchangers.

References

[1] F. Garcia-Moreno, "Commercial Applications of Metal Foams: Their Properties and Production", *Materials*, 9, 85; doi:10.3390/ma9020085, 2016.

[2] T.J. Lu, H.A. Stone and M.F. Ashby, "Heat transfer in open-cell metal foams", *Acta Materialia*, 46(10), 3619-3635, 1998.

[3] K. Boomsma, D. Poulikakos and F. Zwick, "Metal foams as compact high performance heat exchangers", *Mechanics of Materials*, 35, 1161-1176, 2003.

[4] A. Kopanidis, A. Theodorakakos, E. Gavaises and D. Bouris, "3D Numerical simulation of flow and conjugate heat transfer through a pore scale model of high porosity open cell foam", *Int. Journ. of Heat and Mass Transfer*, 53, 2539-2550, 2010.

[5] H. Wang, L.J. Guo and K. Chen, "Theoretical and experimental advances on heat transfer and flow characteristics of metal foams", *Sci. China Tech. Sci*, 63, 705-718, 2020.

[6] S. Meinicke, T. Wetzel and B. Dietrich, "CFD Modeling of single-phase hydrodynamics and heat transfer in solid sponges", *11th Int. Confer. on CFD in the Minerals and Process Industry-CSIRO*, Melbourne, Australia, 7-9 December 2015.

[7] T. Dixit and I. Ghosh, "Simulation intricacies of open-cell metal foam fin subjected to convective flow", *App. Thermal Engin.*,137, 532-544, 2018

[8] A. Jafarizade, M. Panjepour, M. Meratian and M.D. Emami, "Numerical simulation of gas/solid heat transfer in metallic foams: A general correlation for different porosities and pore sizes", *Transport in porous media*, 122(3), DOI 10.1007/s11242-018-1208-x, 2018.

[9] A.M Bayomy. and M.Z. Saghir, "Experimental and numerical study of aluminium metal foam (with/without channels) subjected to steady water flow", *Pertanika Journal of Science and Technology*, **25**(1), 221-246, 2017.

[10] B. Bidar, F. Shahraki and D. M. Kalhori, "3D Numerical modelling of convective heat transfer through two-sided vertical channel symmetrically filled with metal foams", *Periodica Polytechnica Mech. Engineer*., 60(4), 193-2012, 2016.

[11] M. Odabaee and K. Hooman, "Metal foam heat exchangers for heat transfer augmentation from a tube bank", *App. Thermal Engin.*, 36, 456-463, 2012.

[12] S. Mancin, C. Zilio, A. Cavallini and L. Rossetto, "Heat transfer during air flow in aluminum foams", *Int. Journ. of Heat and Mass Transfer*, 53, 4976-4984, 2010.

[13] A.M. Hassan, A.A. Alwan and H.K. Hamzah, "Numerical study of fan coil heat exchanger with copper-foam", *Int. Journ. of Fluid Machinery and Systems*, 16 (1), January-March, 2023.

[14] K. Yang, K. Liu and J. Wang, "Pore-scale numerical simulation of convection heat transfer in high porosity open-cell metal foam under rotating conditions", *Applied Thermal Engineering*, 195, 117168, 2021.

[15] B. Pulvirenti, M. Celli and A. Barletta, "Flow and convection in metal foams: A survey and new CFD results", Fluids, 5, 155; doi:10.3390/ fluids5030155, 2020.

[16] K. Kumar, B. Kotresha and K. Naik, "Flow and heat transfer irreversibility in partial filled metal foams", *Int. Journ. of Thermal Sciences*, 184, 107968, 2023.

[17] N. H. Roge, K. Yogi, A. Singh, H. Shrigondekar, S. Krishnan and S.V. Prabhu, "Local heat transfer distribution of thermally developing region in a rectangular open-cell metal foamed channel", *Int. Journ. of Thermal Sciences*, 203, 109138, 2024.

[18] Comsol AB, Comsol Multiphysics-CFD Module, *User's Guide*, Version 6.2, 2023.

[19] Comsol AB, Comsol Multiphysics-Heat Transfer Module, *User's Guide*, Version 6.2, 2023.

[20] T.L. Bergman, A.S. Lavine, F.P. Incropera and D.P. Dewitt, *Fundamentals of heat and mass transfer*, 7 ed., John Wiley and Sons, Hoboken (NJ), USA, 2011.

Acknowledgements

The authors gratefully acknowledge the financial aid provided by the *Vicerrectoría de Investigación y Extensión of the Instituto Tecnológico de Costa Rica*, through the project 5402-1351-2301 and Eng. Moises Morera A. for the experimental work in the laboratory.